Structure
Article

A Motif in the Vertebrate Telomerase N-Terminal Linker of TERT Contributes to RNA Binding and Telomerase Activity and Processivity

Michael Harkisheimer,[1,3] Mark Mason,[1,2,3] Elena Shuvaeva,[1,2] and Emmanuel Skordalakes[1,2,*]
[1]The Wistar Institute, 3601 Spruce Street, Philadelphia, PA 19104, USA
[2]Department of Chemistry, University of Pennsylvania, Philadelphia, PA 19104, USA
[3]These authors contributed equally to this work
*Correspondence: skorda@wistar.org
http://dx.doi.org/10.1016/j.str.2013.08.013

SUMMARY

Telomerase is a ribonucleoprotein reverse transcriptase that replicates the ends of chromosomes, thus maintaining genome stability. Telomerase ribonucleoprotein assembly is primarily mediated by the RNA binding domain (TRBD) of the enzyme. Here we present the high-resolution TRBD structure of the vertebrate, *Takifugu rubripes* (*tr*TRBD). The structure shows that with the exception of the N-terminal linker, the *tr*TRBD is conserved with the *Tribolium castaneum* and *Tetrahymena thermophila* TRBDs, suggesting evolutionary conservation across species. The structure provides a view of the structural organization of the vertebrate-specific VSR motif that binds the activation domain (CR4/5) of the RNA component of telomerase. It also reveals a motif (TFLY) that forms part of the T-CP pocket implicated in template boundary element (TBE) binding. Mutant proteins of conserved residues that consist of part of the T and TFLY motifs disrupt *tr*TRBD-TBE binding and telomerase activity and processivity, supporting an essential role of these motifs in telomerase RNP assembly and function.

INTRODUCTION

Telomeres are nucleoprotein complexes that serve to protect and maintain the integrity of the ends of chromosomes (Baumann et al., 2002; Blackburn and Gall, 1978; Grandin et al., 2001; Miyake et al., 2009; Song et al., 2008). Telomerase, the enzyme that replicates telomeres, is a stable ribonucleoprotein (RNP) reverse transcriptase consisting of a protein (TERT) that comprises the catalytic subunit of the enzyme and a large RNA component (TER), which contains the template TERT uses to replicate telomeres (Blackburn, 2000; Lamond, 1989; Miller and Collins, 2002; Shippen-Lentz and Blackburn, 1990). TERT is evolutionarily conserved across species with a high degree of conservation within a family of organisms. Differences across species primarily localize to the N-terminal portion of the protein. The most notable difference is the absence of the TEN domain from insects and worms and the diversity of the linker connecting it to the TRBD (Malik et al., 2000; Osanai et al., 2006). The core TERT protein consists of four distinct domains, including the RNA binding domain (TRBD), which is involved in telomerase RNP assembly, template boundary definition, and repeat addition processivity (Cunningham and Collins, 2005; Lai et al., 2002; Miller et al., 2000). Structures of the *Tetrahymena thermophila* and *Tribolium castaneum* TRBD (*tt*TRBD and *tc*TRBD, respectively) revealed an almost all helical nucleic acid binding fold containing several conserved motifs implicated in TER binding (Bley et al., 2011; Bryan et al., 2000; Lai et al., 2001; Moriarty et al., 2002; O'Connor et al., 2005). These include the T and CP motifs, which localize at the interface of the TRBD and fingers domains of TERT. The two motifs are located adjacent to each other and form an extended pocket (T-CP pocket) on the surface of the protein implicated in TBE binding (Gillis et al., 2008; Rouda and Skordalakes, 2007). In vertebrates, additional contacts between TERT and TER are mediated by the VSR motif, a conserved element of the vertebrate N-terminal linker of TERT (Moriarty et al., 2002), which binds the activation domain of TER (Bley et al., 2011).

Here, we present the structure of the vertebrate *tr*TRBD, which has high sequence identity to the human enzyme. The structure provides evidence of structural conservation of the core TRBD across species. It also reveals the structural organization of the conserved portion of the N-terminal linker of vertebrate TRBDs, which contains motifs implicated in TER binding. These include the VSR motif, which binds the activation domain of TER (CR4/5) and a motif (TFLY), which contributes to the T-CP pocket formation and TBE binding. We also show that mutations of conserved residues that form part of the T-TFLY pocket disrupt TBE binding and reduce telomerase processivity.

RESULTS

Structure of the trTRBD Domain

We engineered a telomerase, *tr*TRBD construct consisting of residues 294–545, initially based on sequence alignment and structure prediction software the boundaries of which were subsequently confirmed by limited proteolysis of the TEN-TRBD N-terminal portion of *tr*TERT (Kelley and Sternberg, 2009; Larkin et al., 2007). The construct contains the core TRBD domain of telomerase and the conserved region of the vertebrate

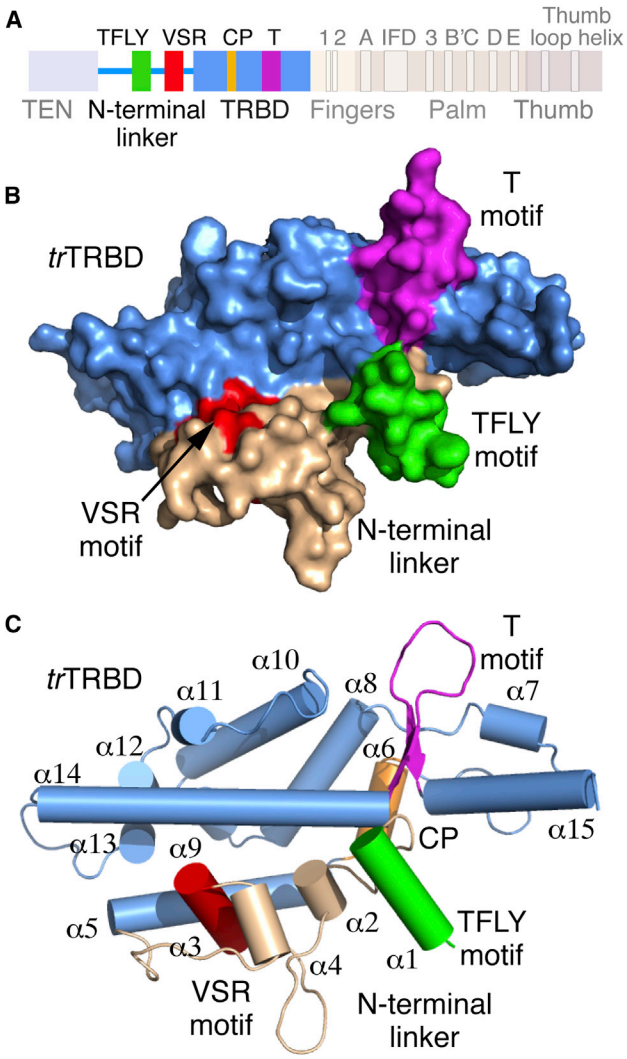

Figure 1. Primary and Tertiary Structure of Vertebrate TRBD and N-Terminal Linker

(A) Primary structure of vertebrate TERT highlighting the TRBD and N-terminal linker motifs.

(B) Surface representation of the three-dimensional structure of the *Takifugu rubripes* TRBD (*tr*TRBD) and conserved portion of the N-terminal linker. The N-terminal linker (wheat), and the TFLY (green), T (magenta), and VSR (red) motifs are shown.

(C) Cartoon representation of the *tr*TRBD shows the N-terminal linker and TFLY, T, and VSR motifs in the same orientation and color as in (B).

Table 1. Data Collection, Phasing, and Refinement Statistics

		Phasing		
	Native	Hg Derivative 1	Hg Derivative 2	Native
Data Collection				
Wavelength (Å)	1.1	1.008	1.008	1.1
Space group	$P2_1$	$P2_12_12_1$	$P2_12_12_1$	$P2_12_12_1$
Cell Dimensions				
a, *b*, *c* (Å)	48.6, 84.5, 137.2	48.8, 84.6, 139.2	48.6, 84.7, 138.8	48.7, 84.7, 139.4
α, β, γ (°)	94.3			
Resolution (Å)	40–2.37 (2.51–2.37)[a]	40–3.4 (3.58–3.4)	40–3.3 (3.48–3.30)	40–3.0 (3.16–3.0)
R_{sym} or R_{merge}	7.0 (32.0)	13.2 (38.9)	18.9 (41.5)	8.4 (39.9)
$I/\sigma I$	9.5 (2.3)	9.7 (2.7)	9.7 (2.1)	13 (2.5)
Completeness (%)	98.6 (92.3)	99.7 (99.6)	97.3 (91.1)	99.4 (99.2)
Redundancy	3.0 (2.4)	3.1 (3.2)	3.3 (3.0)	3.0 (3.0)
Phasing Analysis				
Resolution (Å)	–	–	–	40–3.5
Number of sites	–	–	–	4
Z score	–	–	–	20
Mean figure of merit	–	–	–	0.50
Refinement				
Resolution (Å)	40–2.37	–	–	–
No. reflections	42,409	–	–	–
R_{work}/ R_{free}	21.9/25.8	–	–	–
No. of Atoms				
Protein	8,446	–	–	–
Water	148	–	–	–
B-Factors				
Protein	35.2	–	–	–
Water	37.6	–	–	–
Rmsds				
Bond lengths (Å)	0.005	–	–	–
Bond angles (°)	0.943	–	–	–
Ramachandran Plot (%)				
Most favored	91.5	–	–	–
Allowed	8.5	–	–	–

[a]Values in parentheses represent highest resolution shell.

N-terminal linker that connects it to the TEN domain (Figure 1A). We subsequently solved the structure of *tr*TRBD to 2.37 Å resolution using a single mercury derivative and the method of single isomorphous replacement with anomalous signal (SIRAS; Table 1). The structure, which revealed density for the entire construct, is an elongated helical bundle (Figures 1B and 1C) with clear structural homology to the *tc*TRBD and *tt*TRBD (Figures 2A–2F). Earlier structural and biochemical studies of this portion of TERT identified a number of RNA binding elements, which include the universally CP, T, and vertebrate VSR conserved motifs (Bley et al., 2011; Moriarty et al., 2002; Rouda and Skordalakes, 2007; Figures 1B and 1C). As in *tc*TRBD and *tt*TRBD, the *tr*TRBD CP and T motifs localize at the interface of the TRBD and fingers domains, forming an extended pocket on the surface of the protein implicated in TBE binding (Gillis et al., 2008; Rouda and Skordalakes, 2007; Figures 1B and 1C).

The vertebrate conserved portion of the N-terminal linker of *tr*TRBD is comprised of a complex network of loops and four short α helices (Figures 1B and 1C). This portion of TERT is stably anchored on the surface of TRBD via extensive interactions with helices α5 and α14 that form part of the core *tr*TRBD (Figure 1C). In turn, the N-terminal linker creates an extended surface area

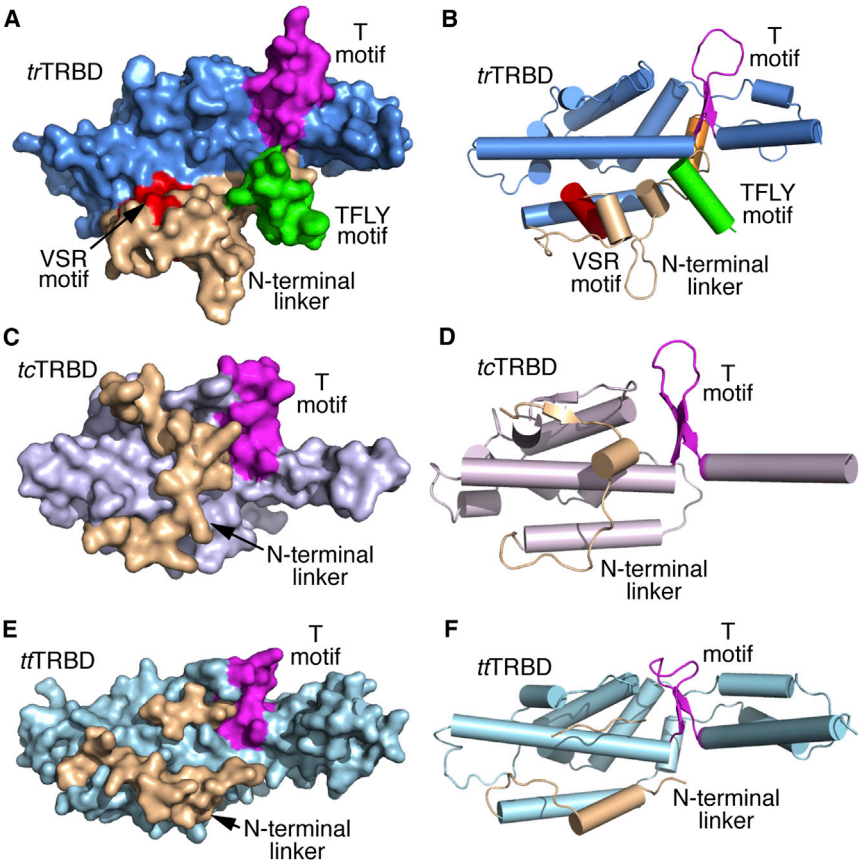

Figure 2. Structural Comparison of the *Takifugu rubripes*, *Tribolium castaneum*, and *Tetrahymena thermophila* TRBD and Portions of Their N-Terminal Linkers

Surface and cartoon representation of *tr*TRBD (A and B), *tc*TRBD (C and D), and *tt*TRBD (E and F) showing the N-terminal linker (wheat), and the T (magenta) and TFLY (green) motifs.

that contains several conserved and solvent accessible residues that may be important for TER binding. For example, the VSR motif is a short helix (α4) that sits perpendicular to helices α5 and α14, which run parallel to each other and span the length of the core of this domain. Interestingly, part of helix α4 is buried under the coils and helices flanking the VSR motif with conserved residues shown to bind CR4/5 (Bley et al., 2011) partially solvent-exposed for RNA binding.

Another interesting feature of the *tr*TRBD N-terminal linker is a short α helix (α1) located upstream of the VSR motif (Figures 1B and 1C). Interestingly, α1 is located in proximity to the CP and T motifs, thus contributing to the formation of the previously identified T-CP pocket (Figures 1B and 1C) and proposed to bind the TBE (Rouda and Skordalakes, 2007). We will refer to it as the TFLY motif after the conserved residues (TxxFLY) that comprise this structural element.

trTRBD and CR4/5 Binding

The Chen lab recently identified three vertebrate conserved residues (F339, W461, and Y486 in *tr*TRBD; Figures 3A and 3B) on the surface of *Oryzias latipies* TRBD (*ol*TRBD), a close structural homolog of *tr*TRBD, involved in CR4/5 binding (Figure S1B available online; Bley et al., 2011). F339 (F355 in *ol*TERT), which forms part of the VSR motif, is partially buried making extensive interactions with P352, L355 and P356 of the coil that connects α4 with α5 as well as F359 of helix α5 (Figure 3B). However, part of F339 is solvent accessible for contacts with the incoming nucleotide of CR4/5. W461 (W477 in *ol*TERT) forms part of the linker that connects helices α11 and α12 (Figure 3B) and is located in proximity to the interface of the TRBD-thumb domain of TERT (Gillis et al., 2008; Mitchell et al., 2010). The third residue, Y486 (Y503 in *ol*TERT), is located toward the N-terminal portion of helix α14 and is centered between F339 (16.8 Å) and W461 (16.5 Å; Figure 3B). Together the three residues form an extensive protein-CR4/5 binding surface that spans the entire width of the TRBD.

trTRBD and TBE Binding

We had previously proposed that the T and CP motifs of *tt*TRBD are involved in TBE binding (Rouda and Skordalakes, 2007). The structure presented here shows that the TFLY motif comprises part of the T-CP pocket and contains several conserved and solvent accessible hydrophobic residues for TBE binding (Figure 3C). To test this hypothesis, we engineered a host of single and double alanine mutants of conserved and solvent exposed residues of the T (Y512A, E514A, E515A, Y512A/T514A, and T514A/E5151A) and TFLY (Y305A) motifs (Figures 3A and 3C). We expressed and purified the proteins to homogeneity (Figure 4A) and tested their ability to bind the TBE (Figures 4B and 4C; Table S1) using fluorescence polarization (FP; Figures 4D and 4E) and electrophoretic mobility shift (EMSA) (Figures S1C–S1K) assays in the presence of 30-fold excess of cold tRNA competitor. We also tested the recombinant *tr*TRBD for CR4/5 (Table S1) binding as a control (Figure S1B). The wild-type (WT) *tr*TRBD had a K_d of ~24 nM for the TBE, whereas the mutant proteins displayed an overall 1.9- to 4.9-fold reduction in TBE binding (Figure 4E). The Y305A mutant and deletion of the TFLY motif showed a 2.5- and 3.5-fold reduction in TBE binding, respectively, suggesting that additional residues of this motif, other than Y305, are involved in TERT-TER association. For example, the vertebrate conserved T300, F303, and L304 residues (Figure 3A) of the TFLY motif face away from the T-CP-TFLY pocket, forming a solvent exposed hydrophobic patch on the surface of the protein, which may be involved in protein or nucleic acid binding. Mutations of residues that comprise the T motif (Y512A, T514A, and E515A) also showed an approximate 2-fold reduction in affinity for TBE. The least effect was observed for the E515A mutant (1.9-fold), which forms part of the T motif and is most proximal to the interior cavity of the TERT ring and

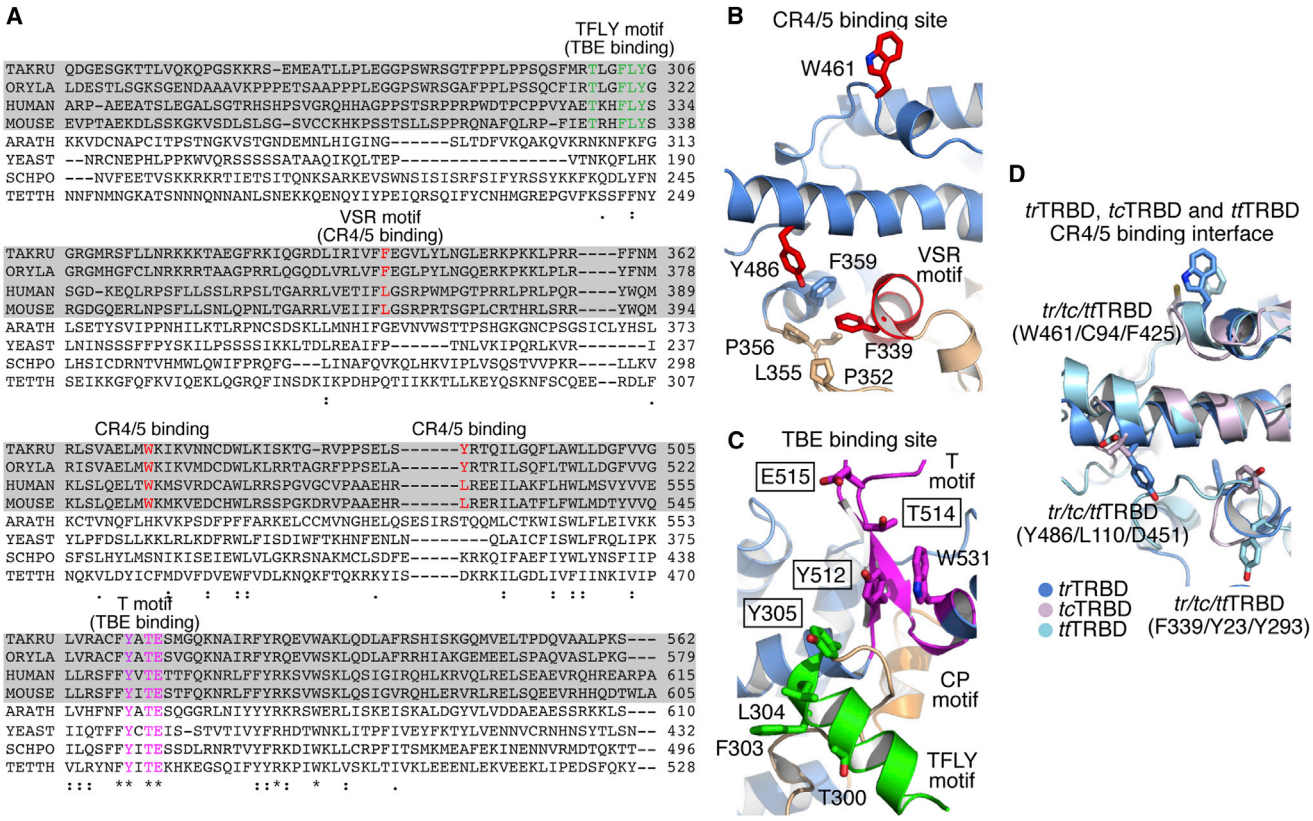

Figure 3. TRBD and N-Terminal Linker Sequence and Structural Conservation

(A) Sequence alignment of the N-terminal linker and TRBD is shown with the conserved TFLY (green), VSR (red), and T (magenta) motifs. The vertebrate sequences are highlighted in gray.

(B and C) Portions of the *tr*TRBD structure highlighting the VSR (red) and adjacent residues involved in CR4/5 binding (B) and the T (magenta) and TFLY (green) motifs involved in TBE binding (C). Conserved residues mutated in this study are shown in boxes.

(D) Structural overlay of the *tr*TRBD (blue), *tt*TRBD (cyan), and *tc*TRBD (violet) CR4/5 binding surface showing structural and amino acid conservation.

where the active site of the enzyme is located (Gillis et al., 2008; Mitchell et al., 2010).

Disruption of trTRBD-TBE Binding Results in Loss of Telomerase Processivity

To test the effects of *tr*TRBD-TBE binding in telomerase function, we assembled the minimal telomerase holoenzyme in vitro using *Escherichia coli* overexpressed WT and mutant (Y305A, Y512A, T514A, E515A, Y512A/E515A, and T514A/E515A) *tr*TERT proteins (Figure 5A) and in vitro transcribed *tr*TER. The proteins were isolated by affinity chromatography and the RNP complex assembled by mixing *tr*TERT with *tr*TER at 1:1 ratio in a buffer containing 25 mM HEPES at pH 7.5, 5% glycerol, 100 mM KCl, and 1 mM TCEP. We then tested the WT and T-TFLY mutant proteins for telomerase activity and processivity using direct assays as described in the Experimental Procedures. The WT in vitro assembled *Takifugu rubripes* telomerase showed robust telomerase activity (Figures 5B and 5C), while the single and double alanine T-TFLY mutant proteins that disrupt TBE binding (Figures 3C, 4D, and 4E) showed significant loss of telomerase activity and processivity (Figures 5B–5D), consistent with the important role of these motifs in telomerase function.

DISCUSSION

Structural Conservation of TRBD

Striking differences in the primary structure of the telomerase protein and RNA subunits have raised significant questions regarding structural and functional conservation of the enzyme across species. For instance, insect and worm TERTs lack the TEN domain, while TERTs of evolutionarily distant species have sequence identity below 20%. Despite these differences, the structure presented here demonstrates that the core of telomerase TRBD is evolutionarily conserved from ciliates to vertebrates with an average root-mean-square deviation (rmsd) of 3.0 Å. The inflated rmsd observed among the *tr*TRBD, *tt*TRBD, and *tc*TRBD is primarily due to the flexibility of the helix (α15) that connects the TRBD to the fingers domain of TERT (Figure 1C). Additional structural differences in the fold of TRBD are observed in the N-terminal region of the protein (Figures 2A–2F), which is the least conserved portion of TERT. For example, insects and worms contain only a portion of this linker, while it is widely variable both in length and sequence even within a family of organisms (Malik et al., 2000). Despite the diversity of the N-terminal linker of telomerase, this structural element is far from merely a passive component of the enzyme. In vertebrates,

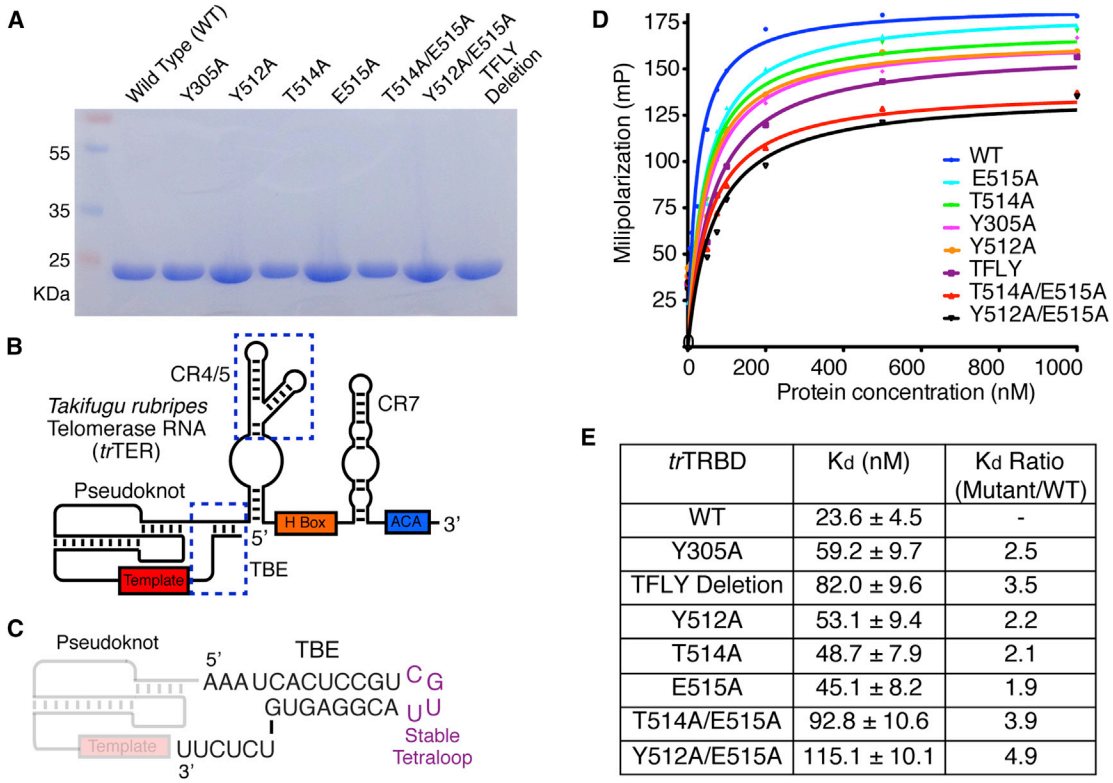

E

*tr*TRBD	Kd (nM)	Kd Ratio (Mutant/WT)
WT	23.6 ± 4.5	-
Y305A	59.2 ± 9.7	2.5
TFLY Deletion	82.0 ± 9.6	3.5
Y512A	53.1 ± 9.4	2.2
T514A	48.7 ± 7.9	2.1
E515A	45.1 ± 8.2	1.9
T514A/E515A	92.8 ± 10.6	3.9
Y512A/E515A	115.1 ± 10.1	4.9

Figure 4. *tr*TER Primary Structure and *tr*TRBD-TBE Binding Data
(A) SDS PAGE gel of the WT and mutant *tr*TRBD proteins used in this study.
(B) Schematic of the *tr*TER RNA showing conserved motifs in color. The CR4/5 and TBE motifs are highlighted with a blue dashed line.
(C) Nucleotide sequence of *tr*TBE used for the FP and EMSAs in this study; the template and pseudoknot regions are also shown as faded.
(D) FP data of the TBE with WT, Y305A, Y512A, T514A, E515A, T514A/E515A, Y512A/E515A, and TFLY deletion *tr*TRBD proteins.
(E) Table of WT and mutant *tr*TRBD-TBE binding constants calculated using Prism5 (GraphPad Software).
See also Figure S1 and Table S1.

the TEN-TRBD linker contains motifs specific to higher eukaryotes, such as the VSR and TFLY, which are involved in RNA binding. It is therefore likely that the N-terminal region of TERT has co-evolved with the RNA component of telomerase to maintain high-affinity binding and stable RNP assembly. The structural and biochemical data presented here provide insights into the role of the vertebrate TERT N-terminal linker motifs VSR and TFLY in TERT-TER binding and telomerase function.

trTRBD CR4/5 Binding and Implications for Telomerase RNP Assembly

The Chen lab showed recently that the vertebrate TRBDs use the VSR motif (F339) and proximal surface exposed residues (W461 and Y486) to bind the activation domain of TER (CR4/5; Bley et al., 2011; Moriarty et al., 2002; Figure 3B). While W461 and F339 are located on opposite ends of the surface of TRBD, Y486 is located at the center of the protein and is equidistant from these two residues. Together, Y486 with W461 and F339 form an extensive and conserved area on the surface of TRBD involved in stable interactions with the activation domain of TER, thus facilitating TERT-TER assembly. Surprisingly, the VSR motif is mostly buried under a network of coils and helices, consisting of several conserved residues among vertebrate telomerases with the F339 partially solvent exposed for CR4/5 binding. The coils and helices of this portion of the N-terminal linker form a structural protrusion on the side of TRBD, located opposite to the TRBD-thumb interface (Figures 6A and 6B). Examination of the surface charge, residue conservation, and the proximity of this portion of the N-terminal linker to the CR4/5 binding site suggests that additional components of this structural element may be involved in RNA or protein (TEN domain) binding. For example, F339 is located near a cluster of conserved and solvent-exposed basic residues, such as R349, K350, K353, and K354, which may be involved in interactions with the backbone of CR4/5. Interestingly, W461 is located adjacent to the TRBD-thumb domain interface of TERT (Figures 6A and 6B; Gillis et al., 2008; Mitchell et al., 2010). The proximity of W461 to the thumb domain suggests that the telomerase RNA and in particular the CR4/5 domain, may also be making contacts with the C-terminal domain of the enzyme. Contacts between TER and the thumb domain may further stabilize the closed TERT ring configuration, a process required for full telomerase activity and processivity.

Despite the low sequence identity of TERT and TER genes and the different structural composition of their N-terminal linker, the CR4/5 binding interface of TRBD appears to be in part

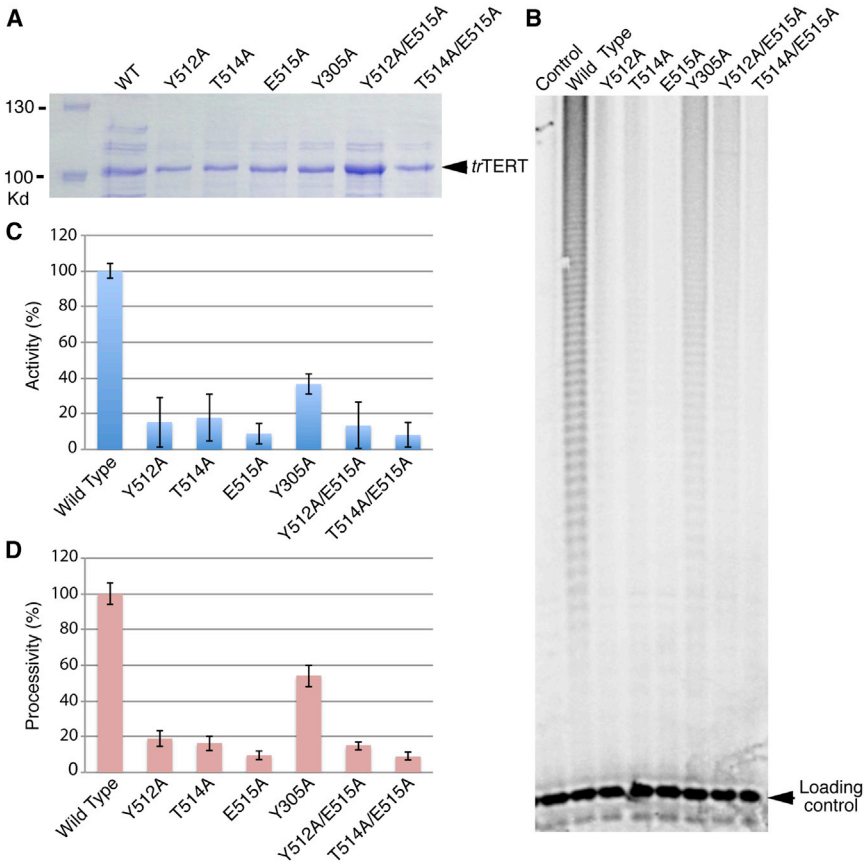

Figure 5. Direct Telomerase Activity Assays of the In Vitro Reconstituted WT and Mutant *tr*TERT Proteins that Disrupt *tr*TRBD-TBE Binding

(A) SDS PAGE gel of WT and mutant *tr*TERT proteins expressed in *E. coli* and used for direct assays with in vitro transcribed RNA.

(B) Direct telomerase activity assays of the WT and mutant *tr*TERTs used in this study.

(C) Percent telomerase activity of mutant *tr*TERT telomerases relative to the WT protein. The percent telomerase activity of each telomerase RNP (WT and mutant *tr*TERT) was measured as the total intensity of all telomeric bands (Using ImageJ), normalized for loading with the intensity of the loading control and divided by the activity of the WT *tr*TERT telomerase.

(D) Percent telomerase processivity of mutant *tr*TERT telomerases relative to the WT protein. The percent telomerase processivity was calculated by measuring the approximate total number of repeats of the WT and mutant telomerase proteins and divided by the total number of WT telomerase repeats. Each experiment was carried out in triplicate, and the error bar represents the SD of the average difference between the three measurements.

conserved across species. For example, structural comparison of *tr*TRBD, *tt*TRBD, and *tc*TRBD shows that the VSR motif, a short helix in vertebrates (Figures 1C and 2B), is a loop in *tc*TRBD (Figures 2C and 2D) and *tt*TRBD (Figures 2E and 2F). However, the proximal spatial position of F339, involved in CR4/5 binding, is occupied in all three structures with Y23 in *tc*TRBD (Figure 3D) and Y293 in *tt*TRBD (Figure 3D). It is therefore possible that Y23 and Y293 of *tc*TRBD and *tt*TRBD, respectively, like F339 of *tr*TRBD, are involved in stacking interactions with an incoming nucleotide of the CR4/5 motif. In contrast, the tertiary structural organization of the W461 and Y368 positions is highly conserved (Figure 3D), while the amino acid composition varies considerably. The W461 of *tr*TRBD is a C94 in *tc*TRBD and a F425 in *tt*TRBD, while Y368 is a L110 in *tc*TRBD and a D451 in *tt*TRBD (Figure 3D). The sequence diversity observed in these two positions could be due to significant differences of the TER nucleotide sequence across species.

The TFLY Motif of Vertebrate TERTs Contributes to T-CP Pocket Formation and TBE Binding

The data presented here provide direct evidence of telomerase TRBD-TBE binding a process mediated by the universally and vertebrate conserved T-CP and TFLY motifs respectively. A host of additional structural and biochemical data support T-CP-TFLY/TBE binding, an interaction important for telomerase assembly, template boundary definition, and repeat addition processivity. For example, the structure of the *tc*TERT-RNA/DNA complex showed that the 5′ end of the RNA template is located at the entry of the T-CP pocket, which positions the TBE within coordinating distance of the T and CP motifs (Figures 6A and 6B; Mitchell et al., 2010). Mutations of conserved residues in the T and CP motifs resulted in reduced full-length TER binding and telomerase activity and processivity (Bryan et al., 2000; Friedman and Cech, 1999; Lai et al., 2002; Moriarty et al., 2002). Moreover, the recent EM structure of *Tetrahymena thermophila* telomerase supports T-CP/TBE binding (Jiang et al., 2013). The identified TFLY motif is a short helix positioned above the CP pocket and forms an extension of the T motif. The organization and residue composition of the TFLY motif creates an extended channel on the surface of TRBD (Figures 1B, 1C, 6A, and 6B). The width and chemical composition of this channel suggest that this portion of TRBD is most likely involved in binding the single stranded RNA portion of TBE (Figure 4C). Single and double alanine mutants of conserved residues that form the T and TFLY motifs partially disrupt TBE binding (Figures 4D, 4E, and S1C–S1K), which suggests that the T, CP, and TFLY motifs act in concert for proper TBE binding. Interestingly, the CP2 motif of ciliate telomerases, also present within the N-terminal linker of the protein, was recently shown to localize in proximity to the T-CP pocket and being involved in TBE binding (Akiyama et al., 2013). As we proposed previously the double-stranded stem loop of the TBE would fit into the electropositive groove formed by the CP motif (Rouda and Skordalakes, 2007). The interaction of the CP motif with the stem loop would position the single-stranded portion of the TBE into the pocket formed by the TFLY and T motifs. Within this pocket, there is a series of several conserved aromatic residues, such as the F303, Y305 of the TFLY, and the Y512 and W531 of the T motifs (Figure 3C), which likely form

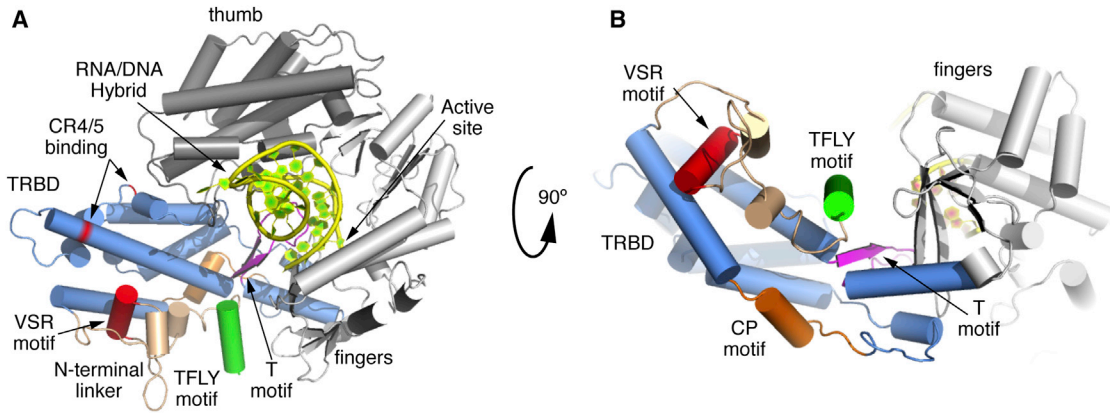

Figure 6. Model of *tc*TERT and *tr*TRBD Showing the Structural Organization of the N-Terminal Linker and TFLY Motifs in the Context of the TERT Ring

(A) Structural overlay of the *tr*TRBD with the *Tribolium castaneum* TERT structures (cartoon). The model shows the structural organization of the CR4/5 (VSR, W461, and Y368; red) and TBE (T and TFLY motifs; magenta and green, respectively) binding interfaces. It shows the RNA/DNA hybrid (yellow) docked in the interior cavity of the TERT ring. It also shows the position of the T motif with respect to the active site of the enzyme.

(B) Same as in (A) rotated 90° along the *x* axis.

base-stacking interactions with the TBE. Interestingly, the T and TFLY motif mutants show modest disruption of TBE binding, suggesting that these residues may have more of a regulatory role in telomerase function. This is consistent with our direct assays, which show that single and double alanine mutants of these residues undergo significant loss of telomerase activity and processivity (Figures 5B and 5C). A striking example is the single alanine mutant E515A. While this mutant showed almost WT TBE binding (1.9-fold; Figures 4D, 4E, S1D, and S1H), it resulted in almost complete loss of telomerase activity and processivity (Figures 5C and 5D). E515A is an invariant residue, located near the tip of the T-motif, which extends toward the interior cavity of the TERT ring and is in proximity to the active site of the enzyme (Figures 6A and 6B). It is therefore possible that this residue and its interaction with the single-stranded portion of the TBE guide the RNA template toward the active site of the enzyme (Gillis et al., 2008; Mitchell et al., 2010). Elimination of the E515-TBE interaction would misplace the RNA template, thus affecting telomerase activity and processivity. We therefore propose that the T and TFLY motifs are important effectors of telomerase activity and processivity by guiding the RNA template into the interior cavity of the TERT ring where the active site of the enzyme is located for nucleotide binding and selectivity.

EXPERIMENTAL PROCEDURES

Construct Design and Protein Expression and Purification

We identified a stable construct of *T. rubripes* TRBD via limited proteolysis of the full-length N-terminal portion of *tr*TERT. We subsequently cloned the *tr*TRBD construct consisting of residues 294–545 in a modified version of the pET28b vector expressing a hexahistidine tag followed by a TEV cleavable small ubiquitin-like modifier (SUMO) fusion protein at its N terminus. We overexpressed the protein in BL21-CodonPlus(DE3)-RIPL cells (Stratagene) for 5 hr at 20°C. We lysed the cells via sonication and purified the protein using Ni-NTA resin (QIAGEN), followed by TEV cleavage of the His-SUMO tag. We further purified the protein to homogeneity using Poros HS (PerSpective Biosystems) and a Superdex S200 size exclusion chromatography (GE Healthcare).

Protein Crystallization and Data Collection

For crystallization studies, we concentrated the purified *tr*TRBD to ~15 mg/ml and dialyzed it in a buffer containing 5 mM Tris-HCl, 200 mM KCl, and 1 mM TCEP (pH 7.5) prior to crystallization trials. Sparse matrix crystal screening using the Hampton Research crystal screens produced two crystal forms (Natrix condition G1) that belong to the $P2_1$ and $P2_12_12_1$ space groups and diffracted to 2.37 Å and 3.0 Å resolution, respectively. Data were collected at the National Synchrotron Light Source, beamline X25, and processed with MOSFLM as implemented in Elves. Phases were calculated using the method of single isomorphous replacement with anomalous signal (SIRAS) and a mercury derivative ($MeHgCl_2$). We located the heavy atom sites, calculated phases, and built a partial model in SOLVE (Brünger et al., 1998) using 4-fold noncrystallographic symmetry. The protein model was subsequently completed manually in COOT (Emsley and Cowtan, 2004) and refined in REFMAC5 (Murshudov et al., 2011). Structural overlays were performed in COOT and figures were made in PyMOL (http://www.pymol.org/).

Electrophoretic Mobility Shift Assays

The TBE and CR4/5 RNA substrates (Table S1) were purchased from Dharmacon and were ^{32}P labeled using 10 μCi/μl of γ-ATP and T4 polynucleotide kinase (New England Biolabs). The WT and mutant *tr*TRBD proteins were incubated with 30 nM cold tRNA (Life Technologies; Ambion yeast tRNA) competitor and 5 μg BSA for 30 min prior to addition of 1 nM of the ^{32}P-labeled TBE to increasing concentrations of protein on ice and in a buffer containing 20 mM Tris-HCl (pH 8.0), 100 mM KCl, 2 mM dithiothreitol (DTT), 1 mM $MgCl_2$, 5% glycerol, 1 mM EDTA, and 0.01% Triton X-100 for 30 min. *tr*TRBD concentrations were calculated using a standard Bradford assay as follows: 50 μl of samples were added to 1.5 ml of Bradford dye and absorbance was measured at absorption at 600 nm. Results of the Bradford assay were corroborated with UV spec at absorption at 260 nm. The reactions were then loaded onto 6% DNA retardation PAGE gels (Invitrogen) and run at 100V for 1 hr. The gels were vacuum-dried and exposed using a storage phosphor screen (GE Healthcare).

Fluorescence Polarization

We performed FP, *tr*TRBD-TBE binding reactions in 15 μl samples using a Wallac EnVision Plate reader (PerkinElmer). The binding reactions were carried out in a buffer containing 20 mM Tris-HCl (pH 8.0), 100 mM KCl, 2 mM $MgCl_2$, 1 mM EDTA, 2 mM DTT, 5% v/v glycerol, and 30 nM cold tRNA competitor (Life Technologies; Ambion yeast tRNA). The TBE probe was purchased with a 5′–labeled Cy5 tag from IDT. The final probe concentration used was 1 nM, while the *tr*TRBD protein concentration ranged from 0 to 1 μM. The reactions

were incubated at room temperature for 5 minutes and pipetted in triplicate into a black 384 well ProxiPlate (PerkinElmer). The reactions were excited with 650 nm light and the emissions were measured at 690 nm. The milipolarization values were calculated by the Envision operating software (PerkinElmer). The data were fit and the binding constants were determined with a one site binding linear regression model using PRISM 5.0 (GraphPad Software, San Diego CA; http://www.graphpad.com).

trTER In Vitro Transcription and Purification

The full-length *tr*TER gene was cloned into the pBSK vector (Addgene) using the KpnI and SacI restriction enzyme sites. The pBSK vector carrying the *tr*TER gene was linearized using SacI-HF (NEB). We then extracted the linearized plasmid from a 1% agarose gel and further purified it using the QIAquick Gel Extraction kit (QIAGEN). The *tr*TER was in vitro transcribed using a reaction mix containing 1× transcription buffer (Promega) containing 10 μM DTT, 0.01% Triton X-100, 2.2 U inorganic pyrophosphatase, 0.5 mM rNTPs, 1 μg of linearized *tr*TER-pBSK, and 80 U of T7 RNA polymerase (Promega). The transcription reaction mix was incubated at 37°C for 1.5 hr, and then 2.2 U of RNase-free DNase (Promega) was added to the mix and incubated for another hour at 37°C to digest the linear *tr*TER-pBSK plasmid. The transcribed product was purified using Trizol extraction (Invitrogen), and a sample was run on a 1% agarose gel to check for RNA quality.

trTERT Expression and Purification

The *tr*TERT WT and mutant genes were cloned into pET28b vector containing an N-terminal hexahistidine tag followed by a TEV cleavable small ubiquitin-like modifier (SUMO) fusion protein. The *tr*TERT proteins were overexpressed in the Scarab *E. coli* strain (Scarab Genomics) overnight at 14°C. The cells were harvested by centrifugation and lysed by sonication in buffer containing 25 mM Tris-HCl (pH 7.5), 5% glycerol, 0.5 M KCl, 0.1 mM benzamidine, 15 mM imidazole, and 0.1 mM phenylmethyl sulfonyl fluoride. The proteins were purified using Ni-NTA resin (QIAGEN) and samples were run on a 12% SDS-PAGE gel to test expression levels and purity.

Direct Telomerase Activity Assay

We tested the activity and processivity of the in vitro reconstituted WT and mutant telomerase proteins using direct telomerase activity assays. The concentration of the Ni-NTA purified *tr*TERT proteins used in each assay was normalized by first loading equal volumes of the Ni-NTA eluted *tr*TERT samples on a SDS-PAGE gel (Figure 5A), and comparing the protein band intensities using ImageJ. Approximately 2 μl or 0.1 μg of the Ni.NTA-purified *tr*TERT proteins (volume was adjusted so that identical concentrations of *tr*TERT proteins were used in all reactions) were incubated for 1.5 hr at 30°C in 20 μl of direct assay buffer consisting of 0.1 μg *tr*TER, 50 mM Tris-HCl (pH 8.0), 50 mM KCl, 1 mM $MgCl_2$, 5 mM beta-mercaptoethanol, 1 mM spermidine, 1 μM TS primer (5′-AATCCGTCGAGCAGAGTT-3′), 0.5 mM dGTP, 0.5 mM dTTP, 2 μM dATP, and 1.25 μM [α-^{32}P] dATP. Reactions were stopped by adding 100 μl of 5 M NH_4OAc, 20 μg of glycogen, 450 μl of 2-propanol, and 0.5 μl of a 200 nM ^{32}P-labeled loading control (budding yeast telomeric 11-mer substrate). Samples were precipitated for 1.5 hr at room temperature, pelleted by centrifugation, washed with 75% 2-propanol, and dried. Pelleted DNA products were resuspended in 25 μl gel-loading buffer (10 mM Tris-HCl [pH 8.0], 10 mM EDTA, 40% formamide, and 0.05% xylene cyanol) and heat denatured at 95°C for 10 min. Samples were run on a 12% polyacrylamide (19:1), 7 M urea gel and exposed overnight to a phosphor screen for imaging. The percent telomerase activity of each protein (WT and Mutant *tr*TERT) were measured as the total intensity of all telomeric bands, normalized for loading with the intensity of the loading control, and divided by the activity of the WT *tr*TERT. The percent processivity was calculated by measuring the approximate total number of repeats of the WT and mutant telomerase proteins and divided by the total number of WT telomerase repeats.

ACCESSION NUMBERS

The Protein Data Bank accession number for the structure reported in this paper is 4LMO.

SUPPLEMENTAL INFORMATION

Supplemental Information includes one figure and one table and can be found with this article online at http://dx.doi.org/10.1016/j.str.2013.08.013.

ACKNOWLEDGMENTS

This project was funded by the Pennsylvania Department of Health and the NIGMS (5 R01 GM088332-03).

Received: May 10, 2013
Revised: July 10, 2013
Accepted: August 12, 2013
Published: September 19, 2013

REFERENCES

Akiyama, B.M., Gomez, A., and Stone, M.D. (2013). A conserved motif in Tetrahymena thermophila telomerase reverse transcriptase is proximal to the RNA template and is essential for boundary definition. J. Biol. Chem. *288*, 22141–22149.

Baumann, P., Podell, E., and Cech, T.R. (2002). Human Pot1 (protection of telomeres) protein: cytolocalization, gene structure, and alternative splicing. Mol. Cell. Biol. *22*, 8079–8087.

Blackburn, E.H. (2000). The end of the (DNA) line. Nat. Struct. Biol. *7*, 847–850.

Blackburn, E.H., and Gall, J.G. (1978). A tandemly repeated sequence at the termini of the extrachromosomal ribosomal RNA genes in Tetrahymena. J. Mol. Biol. *120*, 33–53.

Bley, C.J., Qi, X., Rand, D.P., Borges, C.R., Nelson, R.W., and Chen, J.J. (2011). RNA-protein binding interface in the telomerase ribonucleoprotein. Proc. Natl. Acad. Sci. USA *108*, 20333–20338.

Brünger, A.T., Adams, P.D., Clore, G.M., DeLano, W.L., Gros, P., Grosse-Kunstleve, R.W., Jiang, J.S., Kuszewski, J., Nilges, M., Pannu, N.S., et al. (1998). Crystallography & NMR system: A new software suite for macromolecular structure determination. Acta Crystallogr. D Biol. Crystallogr. *54*, 905–921.

Bryan, T.M., Goodrich, K.J., and Cech, T.R. (2000). Telomerase RNA bound by protein motifs specific to telomerase reverse transcriptase. Mol. Cell *6*, 493–499.

Cunningham, D.D., and Collins, K. (2005). Biological and biochemical functions of RNA in the tetrahymena telomerase holoenzyme. Mol. Cell. Biol. *25*, 4442–4454.

Emsley, P., and Cowtan, K. (2004). Coot: model-building tools for molecular graphics. Acta Crystallogr. D Biol. Crystallogr. *60*, 2126–2132.

Friedman, K.L., and Cech, T.R. (1999). Essential functions of amino-terminal domains in the yeast telomerase catalytic subunit revealed by selection for viable mutants. Genes Dev. *13*, 2863–2874.

Gillis, A.J., Schuller, A.P., and Skordalakes, E. (2008). Structure of the Tribolium castaneum telomerase catalytic subunit TERT. Nature *455*, 633–637.

Grandin, N., Damon, C., and Charbonneau, M. (2001). Cdc13 prevents telomere uncapping and Rad50-dependent homologous recombination. EMBO J. *20*, 6127–6139.

Jiang, J., Miracco, E.J., Hong, K., Eckert, B., Chan, H., Cash, D.D., Min, B., Zhou, Z.H., Collins, K., and Feigon, J. (2013). The architecture of Tetrahymena telomerase holoenzyme. Nature *496*, 187–192.

Kelley, L.A., and Sternberg, M.J. (2009). Protein structure prediction on the Web: a case study using the Phyre server. Nat. Protoc. *4*, 363–371.

Lai, C.K., Mitchell, J.R., and Collins, K. (2001). RNA binding domain of telomerase reverse transcriptase. Mol. Cell. Biol. *21*, 990–1000.

Lai, C.K., Miller, M.C., and Collins, K. (2002). Template boundary definition in Tetrahymena telomerase. Genes Dev. *16*, 415–420.

Lamond, A.I. (1989). Tetrahymena telomerase contains an internal RNA template. Trends Biochem. Sci. *14*, 202–204.

Larkin, M.A., Blackshields, G., Brown, N.P., Chenna, R., McGettigan, P.A., McWilliam, H., Valentin, F., Wallace, I.M., Wilm, A., Lopez, R., et al. (2007). Clustal W and Clustal X version 2.0. Bioinformatics *23*, 2947–2948.

Malik, H.S., Burke, W.D., and Eickbush, T.H. (2000). Putative telomerase catalytic subunits from Giardia lamblia and Caenorhabditis elegans. Gene *251*, 101–108.

Miller, M.C., and Collins, K. (2002). Telomerase recognizes its template by using an adjacent RNA motif. Proc. Natl. Acad. Sci. USA *99*, 6585–6590.

Miller, M.C., Liu, J.K., and Collins, K. (2000). Template definition by Tetrahymena telomerase reverse transcriptase. EMBO J. *19*, 4412–4422.

Mitchell, M., Gillis, A., Futahashi, M., Fujiwara, H., and Skordalakes, E. (2010). Structural basis for telomerase catalytic subunit TERT binding to RNA template and telomeric DNA. Nat. Struct. Mol. Biol. *17*, 513–518.

Miyake, Y., Nakamura, M., Nabetani, A., Shimamura, S., Tamura, M., Yonehara, S., Saito, M., and Ishikawa, F. (2009). RPA-like mammalian Ctc1-Stn1-Ten1 complex binds to single-stranded DNA and protects telomeres independently of the Pot1 pathway. Mol. Cell *36*, 193–206.

Moriarty, T.J., Huard, S., Dupuis, S., and Autexier, C. (2002). Functional multimerization of human telomerase requires an RNA interaction domain in the N terminus of the catalytic subunit. Mol. Cell. Biol. *22*, 1253–1265.

Murshudov, G.N., Skubák, P., Lebedev, A.A., Pannu, N.S., Steiner, R.A., Nicholls, R.A., Winn, M.D., Long, F., and Vagin, A.A. (2011). REFMAC5 for the refinement of macromolecular crystal structures. Acta Crystallogr. D Biol. Crystallogr. *67*, 355–367.

O'Connor, C.M., Lai, C.K., and Collins, K. (2005). Two purified domains of telomerase reverse transcriptase reconstitute sequence-specific interactions with RNA. J. Biol. Chem. *280*, 17533–17539.

Osanai, M., Kojima, K.K., Futahashi, R., Yaguchi, S., and Fujiwara, H. (2006). Identification and characterization of the telomerase reverse transcriptase of Bombyx mori (silkworm) and Tribolium castaneum (flour beetle). Gene *376*, 281–289.

Rouda, S., and Skordalakes, E. (2007). Structure of the RNA-binding domain of telomerase: implications for RNA recognition and binding. Structure *15*, 1403–1412.

Shippen-Lentz, D., and Blackburn, E.H. (1990). Functional evidence for an RNA template in telomerase. Science *247*, 546–552.

Song, X., Leehy, K., Warrington, R.T., Lamb, J.C., Surovtseva, Y.V., and Shippen, D.E. (2008). STN1 protects chromosome ends in Arabidopsis thaliana. Proc. Natl. Acad. Sci. USA *105*, 19815–19820.

